Central European Journal of Energetic Materials
ISSN 1733-7178; e-ISSN 2353-1843

Cent. Eur. J. Energ. Mater., 2016, *13*(4), 927-943; DOI: 10.22211/cejem/65141

A Modified Penetration Model for Copper-Tungsten Shaped Charge Jets with Non-uniform Density Distribution

Tamer ELSHENAWY,[1*] Ahmed ELBEIH,[2] Qing Ming LI [3]

[1] *Technical Research Centre, Cairo, Egypt*
[2] *Military Technical College, Kobry Elkobbah, Cairo, Egypt*
[3] *The University of Manchester, School of Mechanical Aerospace and Civil Engineering, Manchester, UK*
[*] *E-mail: tamershenawy@yahoo.com*

Abstract: The penetration of a shaped charge jet with non-uniform density distribution was studied. The virtual origin model, which assumes a constant jet density, was modified to include the situation where the jet density deficit/reduction of an un-sintered copper-tungsten powder jet causes a non-uniform jet density distribution. A relation between the relative density ratio and the normalised jet velocity is proposed, based on which an analytical solution of the modified virtual origin model is obtained. The validity of the modified virtual origin model was demonstrated by its largely improved prediction in comparison with experimental and numerical results. It showed that the density reduction term reduces the penetration depth by 16.58% for an un-sintered copper-tungsten powder jet.

Keywords: shaped charge, jet penetration, virtual origin, non-uniform density distribution

1 Introduction

Shaped charge jets have an excellent penetration capability into various targets. Thus, it has been successfully used in both military and civilian applications. In these applications, it is necessary to predict the depth of penetration of the shaped charge, which is an important parameter for the assessment of the effect of a shaped charge on a target.

Since a shaped charge jet travels at hypervelocity, the jet-target interaction

can be hydro-dynamically described, and thus a hydrodynamic model [1, 2] can be applied to study the jet's penetration. These original hydrodynamic models assumed uniform distribution of the jet density and the jet velocity along the jet length, and applied the Bernoulli equation at the interface between the jet and target for the pressure equilibrium as shown in Equation 1 and Figure 1, *i.e.*:

$$\frac{1}{2}\rho_j(V_j - U)^2 = \frac{1}{2}\rho_T U^2, \tag{1}$$

where V_j is the impinging velocity of the jet onto the target (observed at the jet/target interface); U is the velocity of the jet-target interface or penetration velocity; ρ_j and ρ_T are the jet density and target density around the jet-target interface, respectively. When the distributions of the jet density and velocity are uniform, the consumption of the jet is controlled by:

$$V - U = -\frac{dl}{dt} \tag{2}$$

where l is the current length of the jet.

The penetration depth, P, of the jet into the target is determined by:

$$U = \frac{dP}{dt} \quad \text{or} \quad P = \int_0^t U dt, \tag{3}$$

where $t = 0$ is the time when the jet starts to hit the target. The maximum penetration depth is reached when the jet is completely consumed at $t = t_f$, or $l(t_f) = 0$. For a jet with an original length of l_0 , the maximum penetration depth is determined by Equations 1-3, *i.e.*:

$$P_{max} = l_0\sqrt{\frac{\rho_j}{\rho_t}}. \tag{4}$$

Equation 4 is also applicable to a solid rod penetrator.

For a particulated jet, the Bernoulli equation cannot be used directly because the internal pressure cannot be supported when the jet is particulated [1]. Since this paper will only consider continuous jets, the interested reader is referred to [2] for the penetration models of particulated jets.

Since the early days of the jet penetration study, it has been realised that the spatial distribution of the jet velocity is not uniform [1]. Birkhoff *et al*. [1] extended the hydrodynamic penetration model (Equation 4) to a jet with non-uniform velocity distribution. However, this model introduced several

parameters that cannot be easily determined, and therefore, it has not been widely used. Abrahamson and Goodier [3] also extended the hydrodynamic penetration model to include a non-uniform jet velocity distribution and the stand-off distance. This model started from an arbitrarily selected initial time and required the initial jet length at this moment to be known, which makes the model difficult to use practically.

The concept of a virtual origin was first proposed by Allison and Bryan [4] and then developed by Allison and Vitali [5] and Schwartz [6] for the penetration of continuous and particulated jets with consideration of the velocity gradient and the stand-off distance between the virtual origin and the target surface. This model has been widely accepted, and can be used to predict the penetration depth before and after jet breakup [2, 7].

The virtual origin model retains the basic equations in the hydrodynamic model, *i.e*. Equations 1 and 3, where the strengths and the compressibility of the jet and target materials are neglected, but considers the jet stretching as it travels forwards. In addition, some assumptions were considered during the penetration calculations in [4, 5]. All of the jet elements are formed simultaneously at a virtual origin, located a distance Z_0 in front of the target surface. Each jet element is emitted from the virtual origin at its own velocity and remains constant during its movement between the virtual origin and the target. The density of each element remains constant during this movement and the spatial distribution of the jet density is uniform. However, it has been observed that there is a density deficit based on flash X-ray measurements and the soft recovery of jet fragments [8, 9]. In addition, variable density distribution was also observed in jets formed from powdered metal liners [10-12]. Therefore, it was necessary to extend the virtual origin model to a jet with non-uniform density distribution.

This paper retains the assumption that the density of each jet element remains constant during its motion, but considers the non-uniform jet density distribution to study its effect on the penetration depth. The non-uniform jet density distribution along its axial distance were estimated numerically using the Autodyn jet formation algorithm for a copper-tungsten un-sintered powder liner. An analytical approach was introduced to account for the penetration decrease due to the non-uniform density distribution along its axis. The proposed model was validated by both experiments and numerical simulations using the Autodyn hydro-code.

2 Penetration Analytical Model

In this paper, we will focus on the jet penetration before breakup. Figure 1 is a schematic drawing that defines the penetration parameters of a shaped charge jet penetrating into an incompressible target. Z_0 is the standoff distance from the virtual origin point to the target surface, t is the penetration time, $P(t)$ is the penetration depth at time t and V_j is the impinging velocity of the jet onto the target (observed at the jet/target interface), which is equal to the velocity of the jet element that impacts the target at the same moment in time t.

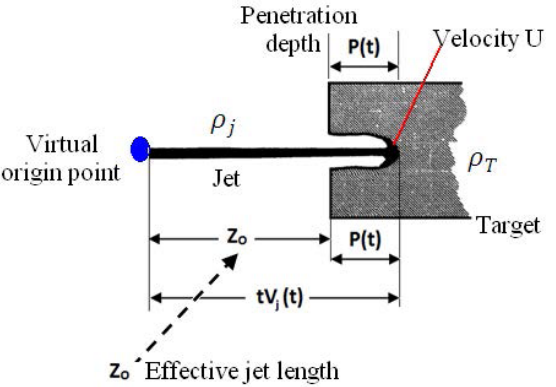

Figure 1. The hydrodynamic jet penetration; [5].

Therefore, the penetration depth $P(t)$ at a given time t is determined by:

$$P(t) = tV_j(t) - Z_0 \tag{5}$$

The depth of penetration increases monotonically with time, which requires the following condition to be satisfied:

$$\frac{dP}{dt} \geq 0 \text{ for } tV_j(t) \geq Z_0 \tag{6}$$

when the hydrodynamic Bernoulli equation (Equation 1) is applied, thus:

$$U = \frac{V_j}{\gamma+1} \tag{7}$$

where $\gamma = \sqrt{\rho_T \ \rho_j}$.

The following Equation 8 can be obtained from Equations 3, 5 and 7:

$$V_j(t) + t\frac{dV_j(t)}{dt} = \frac{V_j(t)}{\gamma+1}. \tag{8}$$

When the jet density is a constant, the solution of Equation 8 predicts the jet velocity $V_j(t)$ as:

$$V_j(t) = V_0\left(\frac{t_0}{t}\right)^{\frac{\gamma}{\gamma+1}} \tag{9}$$

where V_0 is the jet tip velocity and t_0 is the time when the jet tip reaches the target surface (*i.e.* $t_0V_0 = Z_0$).

From Equation 9,

$$t = t_0\left(\frac{V_0}{V_j(t)}\right)^{\frac{\gamma+1}{\gamma}} \tag{10}$$

Therefore, the penetration depth at time t can be obtained from Equation 5 when $V_j(t)$ and t in Equation 5 are substituted by Equations 9 and 10:

$$P(t) = Z_0\left[\left(\frac{V_0}{V_j}\right)^{\frac{1}{\gamma}} - 1\right] = Z_0\left[\left(\frac{t}{t_0}\right)^{\frac{1}{\gamma+1}} - 1\right]. \tag{11}$$

The maximum penetration is achieved at time when the cut-off jet element (*i.e.* the last jet element that has hydrodynamic penetration capability) hits the target at the cut-off velocity (V_c). Therefore, the maximum penetration depth is:

$$P = Z_0\left[\left(\frac{V_0}{V_c}\right)^{\frac{1}{\gamma}} - 1\right]. \tag{12}$$

Equation 12 is called the DSM model (Dipersio, Simon and Merendino), which can also be used to obtain the exit velocity V_P of a continuous jet after perforating a finite thickness (Ti) [2] and takes the form:

$$V_{jex} = V_{jin}\left(\frac{Z_0}{Z_0+T}\right)^{\gamma_i} \tag{13}$$

where V_{jex} and V_{jin} are the exit and the input jet tip velocities, respectively; and

T is the finite target thickness layer to be perforated. Equations 5-13 are well known as the extended hydrodynamic theory of a jet with non-uniform velocity distribution. Detailed discussions about this theory and its derivations can be found in [4-7].

In the currently proposed model, it is assumed that the density of each jet element will remain constant during its movement between the virtual origin and the target. However, since different jet elements have different jet formation processes, their densities are different. Therefore, the spatial distribution of the jet density is non-uniform. At the jet-target interface, the observed jet density should be a function of time, *i.e.* $\rho_j = \rho_j(t)$. If we let the original density of the liner material be represented by ρ_{j0} and the density of the target ρ_T to be a constant, then $\gamma_0 = \sqrt{\rho_T/\rho_{j0}}$ and $\gamma(t) = \sqrt{\rho_T/\rho_j(t)}$. Thus:

$$\frac{\gamma(t)}{\gamma_0} = \sqrt{\frac{\rho_{j0}}{\rho_j(t)}}.$$

Based on the jet formation analysis presented later in Section 5.1, it was found that the normalised jet density is directly related to the normalised jet velocity in a linear relationship, as shown in Figure 2. According to Figure 2, the density deficit/reduction at the jet tip is larger than that at the jet rear. The maximum density reduction in the simulated example was around 20.3% for a copper-tungsten un-sintered liner (at the jet tip). This values agrees with experimental observations [8]. Details of the numerical simulation will be presented in Sections 4 and 5.1.

The linear relationship between $\frac{\gamma(t)}{\gamma_0}$ and $\frac{V_j(t)}{V_0}$ can be described by:

$$\frac{\gamma(t)}{\gamma_0} = a\frac{V_j(t)}{V_0} + b \tag{14}$$

where *a* and *b* are constants to be determined from data fitting of numerical results and analytical considerations, which will be given at the end of this section.

Equation 8 can be rearranged as $\frac{-dV_j}{\mathrm{V_j}(\tau)} - \frac{dV_j}{\gamma(\tau)\mathrm{V_j}(\tau)} = \frac{d\tau}{\tau}$, which can be integrated when Equation 14 is used, *i.e.* $\int_{V_0}^{V_j(t)} \frac{-dV_j}{V_j(\tau)} - \frac{1}{\gamma_0}\int_{V_0}^{V_j(t)} \frac{dV_j}{\mathrm{V_j}(\tau)\left(\frac{a}{V_0}V_j(\tau)+b\right)} = \int_{t_0}^{t}\frac{d\tau}{\tau}$, or

$$t = t_0\left(\frac{V_0}{V_j(t)}\right)^{1+\frac{1}{b\gamma_o}}\left[\frac{\left(\frac{a}{V_0}V_j(t)+\mathrm{b}\right)}{\left(\frac{a}{V_0}V_0+b\right)}\right]^{\frac{1}{b\gamma_o}}. \tag{15}$$

This equation is reduced to Equation 10 when $\frac{\gamma(t)}{\gamma_0} = 1$ or $a = 0$ and $b = 1$ in Equation 14.

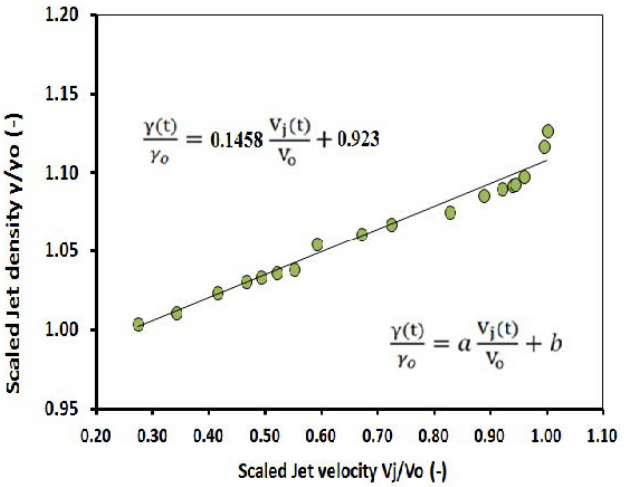

Figure 2. The relationship between the scaled density ratio and the scaled jet velocity; obtained numerically.

When $t = t_c$, $V_j(t) = V_c$, the maximum penetration is achieved by the last penetrating element at a cut-off velocity of V_c; t_c can be determined by Equation 15, *i.e.*:

$$t_c = t_o \left(\frac{V_0}{V_c}\right)^{1+\frac{1}{b\gamma_o}} \left[\frac{\gamma_C}{\gamma_t}\right]^{\frac{1}{b\gamma_o}} \tag{16}$$

where $\gamma_c = \sqrt{\rho_T/\rho_{jc}} = \gamma_0\left(a\frac{V_c}{V_0} + b\right)$ and $\gamma_t = \sqrt{\rho_T/\rho_{jt}} = \gamma_0(a+b)$ according to Equation 14, in which ρ_{jc} and ρ_{jt} are the densities of the last penetrating element and the tip element of the jet, respectively.

From Equation 15, the impact velocity of the jet is determined by an algebraic equation:

$$b\left(\frac{V_0}{V_j}\right)^{b\gamma_0+1} + a\left(\frac{V_0}{V_j}\right)^{b\gamma_0} = (a+b)\left(\frac{t}{t_0}\right)^{b\gamma_0}. \tag{17}$$

Equation 17 reduces to Equation 9 for a constant jet density, when $a = 0$ and $b = 1$.

The penetration depth at time t is determined by Equation 5 when t is substituted from Equation 15

$$P(t) = Z_0 \left[\left(\frac{V_0}{V_j}\right)^{\frac{1}{b\gamma_o}} \left(\frac{a\frac{V_j}{V_o}+b}{a+b} \right)^{\frac{1}{b\gamma_0}} - 1 \right], \tag{18}$$

which can be reduced to Equation 11 for a constant jet density, when $a = 0$ and $b = 1$. The solution of Equation 18 is needed to give an explicit expression of $P(t)$ in Equation 17.

Therefore, the maximum penetration depth is given by:

$$P = Z_0 \left[\left(\frac{V_0}{V_c}\right)^{\frac{1}{b\gamma_o}} \left(\frac{a\frac{V_c}{V_o}+b}{a+b} \right)^{\frac{1}{b\gamma_0}} - 1 \right] = Z_o \left[\left(\frac{V_0}{V_c}\right)^{\frac{1}{b\gamma_o}} \left(\frac{\gamma_c}{\gamma_t}\right)^{\frac{1}{b\gamma_o}} - 1 \right] \tag{19}$$

When $V_j = V_c$ and $t = t_c$, Equation 19 is reduced to Equation 12 for a constant jet density, when $a = 0$ and $b = 1$ or when $\gamma_c = \gamma_t = \gamma_o$ and $b = 1$. The value of a in Equation 14 was determined from curve fitting of the $\gamma - V_j$ relationship along the jet length in Figure 2, which is shown in Table 1.

It was further found that parameter a is correlated with the density of the liner material (ρ_{j0}), the standoff distance ($V_o - V_c$) t, (t is the time taken by the jet tip element from jet formation until it reaches the target surface), the total mass of the jet (m_{jet}) obtained from a standard jetting analysis and the average radius of the jet (r) from a jet formation Autodyn simulation or flash X-ray experiment. A non-dimensional formula can be recommended for the calculation of parameter a, *i.e.*:

$$a = \frac{m_{jet} - \left(\rho_{j0}\ \pi r^2 (V_0 - V_c)\mathrm{t}\right)}{m_{jet}}. \tag{20}$$

The value of a is calculated using Equation 20 for the copper-tungsten liner material and found to be 0.186, but from the curve fitting in Figure 2, it was found to be 0.1458. According to Table 1, the value of b can be approximated to unity for the liner material.

Table 1. The values of parameters a and b in Equation 14

Curve fitting		a (Equation 20)
a	b	
0.1458	0.923	0.186

As in the classic virtual origin (V.O.) model, the jet tip exit velocity perforating a finite thickness target using Equation 19 can be calculated, where a non-uniform density effect is considered. Thus the exit velocity is calculated by:

$$V_{jex} = \frac{bV_{jin}}{(a+b)\left(\frac{Z_0+T}{Z_0}\right)^{b\gamma_i}-a}. \tag{21}$$

3 Experimental

Three un-sintered copper-tungsten powder liners have been used in this study. The liner had a small base diameter of 33 mm, a cone apex angle of 46° and a variable liner wall thickness, as shown in Figure 3. The composition of the powder mixture ingredients are listed in Table 2. This has been tested before and exhibited a good penetration capability, especially at short stand-off distances [13-16]. The powder metallurgy (PM) technique was used to manufacture these liners. A small average grain size with irregular particle shape were chosen for the liner ingredients. The powders were mixed together in the designated mass ratio until a homogeneous mixture blend was obtained, after which they were pressed using an Instron uni-axial hydraulic press. The applied pressure was 100 MPa using the hydraulic press at a low rate (*i.e.* 1 MPa per second) to avoid trapping air voids inside the liner material. The product was a brittle material in the pre-sintering state and was called "the green product", which was tested in this state without sintering as shown in Figure 4. The charge casings were steel with an average wall thickness of 4.5 mm.

Regarding the literature, several types of plastic explosives can be used for filling the charge cases, such as the French plastic explosive named Formex P1 [17] and the American plastic explosive Composition C4 [18-19]. Selection of the plastic explosive was based on performance and sensitivity to different stimuli [20-22]. The main explosive charges for the three charges were PE4 with a total average mass of 24.5 g and a standard deviation of 0.8 g. The British explosive PE4 is a powerful RDX-based plastic explosive (88% RDX plasticized by 9% paraffin oil, 2% lithium stearate and 1% pentaerythritol diolate) [23]. It has a detonation velocity of 8027 m/s at 1.59 g/cm^3 density [24] and 8200 m/s at 1.6 g/cm^3 density [25]. The explosive charge was filled into the steel casing first. Then, the liner was pressed slowly against the steel casing containing the explosive to avoid forming air gaps inside the explosive. The charge was attached to the RHA (Rolled Homogeneous Armour) target and positioned 33 mm away (*i.e.* 1D SOD).

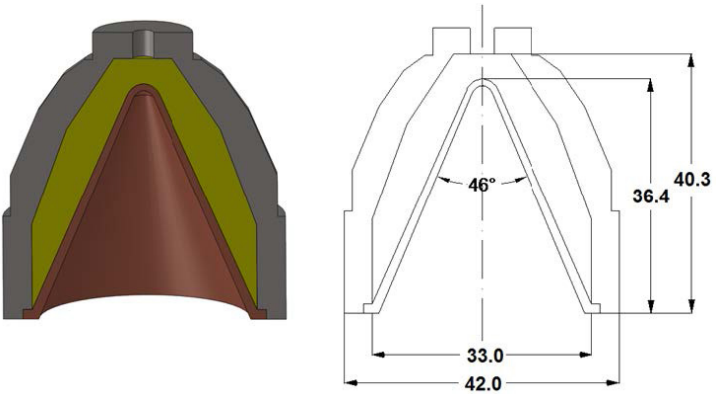

Figure 3. A sketch of the shaped charge design.

Table 2. The mass percentage of the powder liner composition

Material	Copper	Tungsten	Tin	Graphite
Mass [%]	43	45	11	1
Av. grain size [μm]	3	0.6-1	< 45	< 20
Function	binder	main powder	binder coating	lubricant

NOTE : The three tested liners have the same chemical composition, as listed in Table 2.

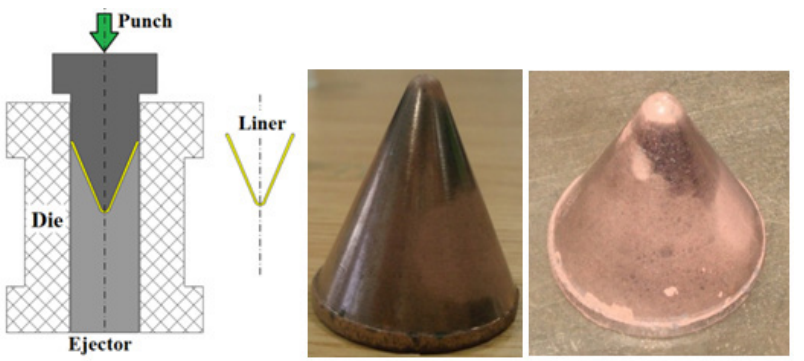

Figure 4. The punch, the die, the ejector and the powder liners produced.

4 Numerical Model Algorithms

Autodyn hydrocode was used in this paper through three algorithms, the Shell jetting analysis, the Euler jet formation and the Lagrange-Lagrange jet penetration model [26].

The jetting analysis was based on the analytically unsteady PER model [27], which is solved numerically using the finite difference technique to calculate the jet and slug velocities, the masses and the collapse and deflection angles of the jet elements. The jetting analysis was validated by comparing the jetting analysis results of a 90 mm shaped charge with actual experimental results [28]. The jet formation modelling was performed using the Euler method based on continuum mechanics to obtain the jet profiles at different times. In this scheme, the explosive, the charge casing and the liner materials are filled into the global Euler multi-material part [29, 30]. This solver is suitable in the early jet formation stages where large distortions are caused by an extremely high strain-rate (*i.e.* $10^7\ s^{-1}$). The evolved jet was allowed to move on the Euler grids up to the moment when the first jet element starts to impact the target. At this point, the formed jet is remapped as a Lagrangian mass having non-uniform velocity and density distributions. It was then exported to the Lagrange jet penetration model for penetration analysis, where both the jet and RHA target are described in the Lagrange method [30].

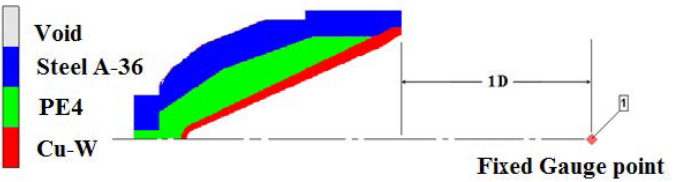

Figure 5. Location of the fixed gauge point used to record the density and the velocity histories.

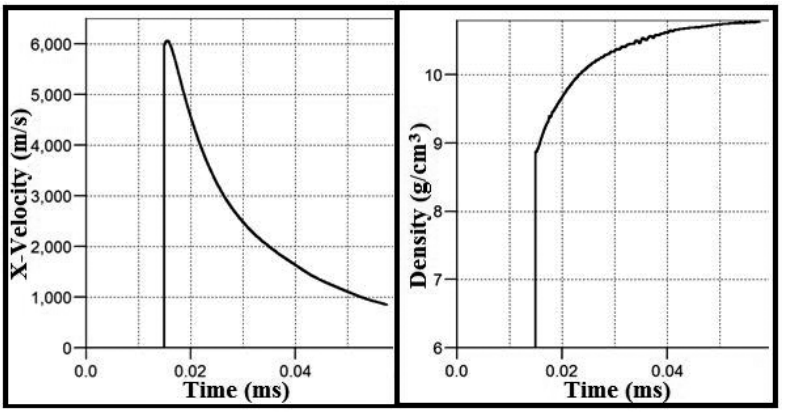

Figure 6. The recorded velocity- and density-time histories for the fixed gauge point.

The mesh sensitivity of the jet characteristics will not be discussed in this paper. However, general uniform 0.50 mm square meshes of the Euler grids were used. A fixed gauge point located at 1 D (one times calibre; *i.e.* 33 mm) was used to record the velocity and density-time histories for the fixed gauge point, as shown in Figure 5. The density of the jet material was found to gradually increase from the tip to the tail due to the existence of a velocity gradient, which clarifies the inverse relation between the jet density and its velocity as shown in Figure 6.

5 Results

5.1 Jet density distribution

The density of the jet along its length was calculated from the jet formation model for the copper-tungsten liner, where a Mie-Gruneisen EOS based on the shock Hugoniot was used. The density of the collapsed liner material is directly related to the liner compressibility and the pressure generated from the explosive load. Distributions of both density and velocity over the entire jet length are depicted in Figure 7 for the copper-tungsten jet. This figure shows that the jet density decreases from slug to tip along the jet. In addition, the density contours also show a radial density distribution on the circular cross-section of the jet (*i.e.* the density at the tip extremity is 9% larger than that at its centreline). Figure 8 shows the velocity and the density histories of the copper-tungsten jet recorded at the fixed gauge point shown in Figure 5.

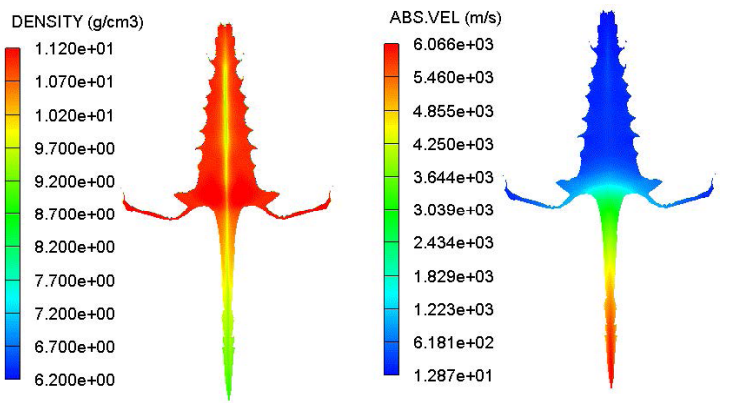

Figure 7. Non-uniform distributions of the Cu-W jet density (left) and jet velocity (right).

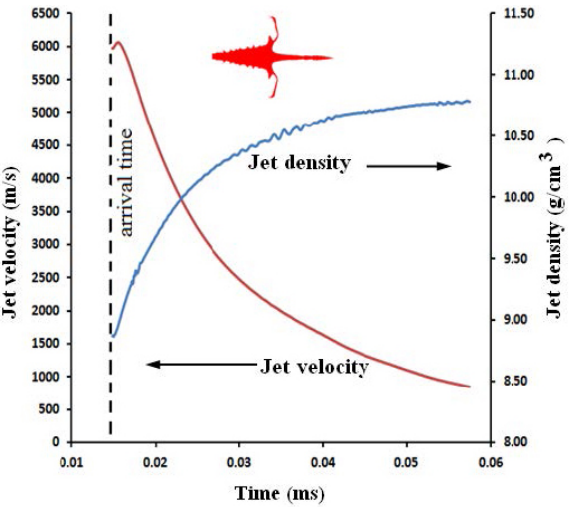

Figure 8. Jet velocity and density histories recorded at the fixed gauge point.

5.2 The penetration depth calculations

The projected effective jet length for the Cu-W shaped charge liner was calculated by back projection of the time-effective jet length fan plot at the moment when the jet reaches the RHA target as shown in Figure 9. The time was determined from the numerical shaped charge jet formation model and was confirmed by calculation using the distance from the virtual origin point to the target front surface; it was found to be at 8.06 μs, which is relevant to the standoff distance of 1D (*i.e.* 33 mm) as illustrated in Figure 5. The relevant effective jet length Z_0 was found to be 4.65 cm.

Equation 19, together with Figure 9, was used to predict the penetration depth of a shaped charge jet into an RHA target when the non-uniform density distribution of the jet is considered. The jet tip and cutoff velocities were obtained from the jetting analysis. Samples of the jetting analysis output are shown in Figure 10 and summarized in Table 3. Figure 10 shows the location of the V.O. point, the initial axial position of the jet elements together and the initial liner position. Back projection of the jet tip and the cut-off elements obtained from the Autodyn standard jet formation algorithm were used further to locate the virtual origin point that is considered the datum point source used to measure the effective jet length from the V.O. point to the target surface as explained in Section 1.

Table 4 presents the penetration depth calculated using various methods, including the modified virtual origin model (Equation 19) from Section 2, the

classic V.O. model, the numerical simulation and the experimental depth of penetration, as well as the penetration reduction due to the density gradient (deficit/reduction).

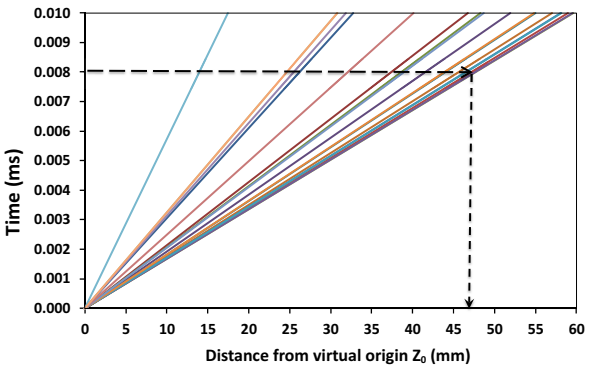

Figure 9. The fan plot of the copper-tungsten jet showing the virtual origin effective jet length at 8.06 μs.

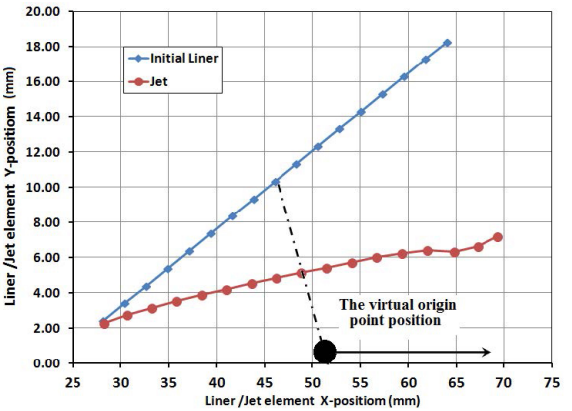

Figure 10. The location of the V.O. point, and the initial and final X-Y positions of the liner and jet elements.

The calculated penetration depth and the percentage reduction in penetration due to the density gradient along the jet length, indicate that the reduction term has a considerable influence on the predicted penetration depth of a shaped charge powder jet. The data in Table 4 are presented in Figure 11. This clearly shows that the modified virtual origin model largely improves predictions of the penetration depth by the virtual origin model for the tested liner type.

Table 3. The jetting data used to estimate the penetration depth

Property	Value
V_{tip} [m/s]	5959
V_{cutoff} [m/s]	1747
Z_0 [cm]	4.65
Solid jet density, ρ_j [g/cm^3]	11.27
Target density, ρ_T [g/cm^3]	7.80
$\gamma = (\rho_t/\rho_j)^{0.5}$	0.83

Table 4. Comparison of the experimental results, the numerical simulations and the virtual origin models' predictions of the penetration of a Cu-W jet

Penetration depth [cm]				Reduction [%]
Exp.	Num. Simulation	Classic V.O. Eq. 12	Modified V.O. Eq. 19	(Classic V.O. – Mod. V.O.) ×100/Classic V.O.
12.8	12.2	15.62	13.03	16.58

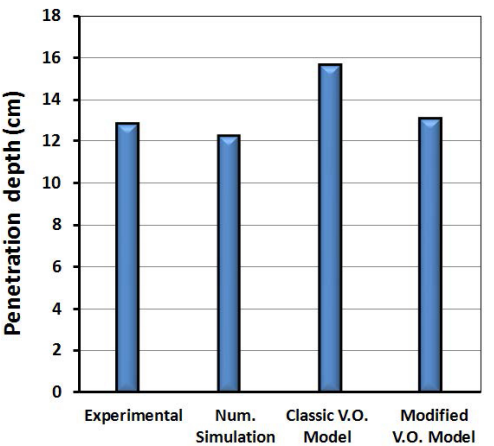

Figure 11. Comparison of the experimental result, the numerical simulation and the virtual origin models' predictions for the penetration of a Cu-W jet.

6 Conclusions

The density deficit/reduction of a shaped charge jet develops during jet formation has been demonstrated experimentally and numerically in this paper. This leads

to the non-uniform distribution of the jet density and consequently the original virtual origin penetration model is incapable of dealing with such a jet with non-uniform density distribution. A correlation between the jet density reduction and the jet velocity is proposed in this paper, based on which an analytical solution of the modified virtual origin model was obtained. The modified virtual origin model shows the penetration depth to be higher than the experimentally measured value by only 1.8%, while the calculation performed by a numerical simulation is lower than the experimentally measured value by 4.7%. The validity of the modified virtual origin model was demonstrated by its largely improved predictions in comparison with the experimental and numerical results.

References

[1] Birkhoff G., Macdougall D.P., Pugh E.M., Taylor G., Explosives with Lined Cavities, *J. Appl. Phys.*, **1948**, *19*, 563.
[2] Walters W.P., Flis W.J., Chou P.C., A Survey of Shaped-charge Jet Penetration Models, *Int. J. Impact Eng.*, **1988**, *7*(3), 307.
[3] Abrahamson G.R., Goodier J.N., Penetration by Shaped Charge Jets of Nonuniform Velocity, *J. Appl. Phys.*, **1963**, *34*(1), 195.
[4] Bryan G.M. Allison F.E., Cratering by a Train of Hypervelocity Fragments, *Proc. 2nd Hypervelocity Impact Effects Symp.*, **1957**, 1.
[5] Allison F.E., Vitali R., *A New Method of Computing Penetration Variables for Shaped Charge Jet*, Ballistic Research Laboratory Report No. 1184, **1963**.
[6] Schwartz W., Modified SDM Model for the Calculation of Shaped Charge Hole Profiles, *Propellants Explos. Pyrotech.*, **1994**. *19*(4), 192-201.
[7] Simon J., Dipersio R., Merendino A.B., *Penetration of Shaped-charge Jets into Metallic Targets*, Ballistic Research Laboratory Memorandum, Report No. 1296, **1965**.
[8] Zernow L., The Density Deficit in Stretching Shaped Charge Jets, *Int. J. Impact Eng.*, **1997**, *20*, 849.
[9] Jamet F., *Measurements of Densities in Shaped Charge Jets and Detonation Waves*, American Society for Non-Destructive Testing, **1976**.
[10] Werneyer K.D., Mostert F.J., Analytical Model Predicting the Penetration Behaviour of a Jet with a Time-varying Density Profile, *21st Int. Symposium on Ballistics*, South Africa, **2004**, 390.
[11] Maritz M.F., Werneyer K.D., Mostert F.J., An Analytical Penetration Model for Jets with Varying Mass Density Profiles, *22nd Int. Symposium on Ballistics*, Canada, **2005**, 622.
[12] Grove B., Walton I., Shaped Charge Jet Velocity and Density Profiles, *23rd Int. Symposium on Ballistics*, Spain **2007**, 103.

[13] Zygmunt B., Wilk Z., Formation of Jets by Shaped Charges with Metal Powder Liners, *Propellants Explos. Pyrotech.*, **2008**, *33*, 482.
[14] Leidel D.J., Lawson J.P., *High Performance Powder Metal Mixtures for Shaped Charge Liners*, Patent US 7,547,345 B2, **2009**.
[15] Yingbin L., Zhaowu S., Numerical Simulation on Formation and Penetration Target of Powder Metal Shaped Charge Jet, *Int. Conf. on Computer Application and System Modelling (ICCASM)*, **2010**, V9-518.
[16] Walters W., Peregino P., Summers R., *A Study of Jets from Un-sintered Powder Metal Lined Non-precision Small Calibre Shaped Charge*, Army Research Lab. Report No. MD 21005-5066, **2001**.
[17] Zeman S., Elbeih A., Yan Q.-L., Note on the Use of the Vacuum Stability Test in the Study of Initiation Reactivity of Attractive Cyclic Nitramines in Formex P1 Matrix, *J. Therm. Anal. Calorim.*, **2013**, *111*, 1503.
[18] Elbeih A., Zeman S., Pachmáň J., Vávra P., Trzciński W.A., Akštein Z., Detonation Characteristics of Attractive Cyclic Nitramines Bonded by Plastic Matrices Based on Polyisobutylene and Poly(methyl methacrylate) Binders, *J. Energ. Mater*., **2012**, *30*(4), 358.
[19] Elbeih A., Jungova M., Zeman, S., Vavra P., Akstein Z., Explosive Strength and Impact Sensitivity of Several PBXs Based on Attractive Cyclic Nitramines, *Propellants Explos. Pyrotech*., **2012**, *37*(3), 329.
[20] Elbeih A., Zeman S., Jungova M., Vavra P., Akstein Z., Effect of Different Polymeric Matrices on Some Properties of Plastic Bonded Explosives, *Propellants Explos. Pyrotech*., **2012**, *37*(6), 676.
[21] Elbeih A., Zeman, S., Pachman J., Effect of Polar Plasticizers on the Characteristics of Selected Cyclic Nitramines, *Cent. Eur. J. Energ. Mater*., **2013**, *10*(3), 339.
[22] Elbeih A., Zeman, S., Jungova M., Akstein Z., Effect of Different Polymeric Matrices on Sensitivity and Performance of Interesting Cyclic Nitramines, *Cent. Eur. J. Energ. Mater*., **2012**, *9*(2), 17.
[23] Thurman J.T., *Practical Bomb Scene Investigation*, 2nd ed., CRC Press, London, **2011**; ISBN 9781439819593.
[24] Chick M.C., Learmonth L.A., *Determination of Shock Initiation and Detonation Characteristics of PE4 in Proof Test Geometries*, Report No. MRL-R-979, **1986**.
[25] Wharton R.K., Formby S.A., Merrifield R., Air blast TNT Equivalence for a Range of Commercial Blasting Explosives, *J. Hazard. Mater.*, **2000**, *79*, 3.
[26] *AUTODYN® Theory Manual*, 3rd Revision, Century Dynamics, USA, **1997**.
[27] Pugh E.M., Eichelberger R.J., Rostoker N., Theory of Jet Formation by Charges with Lined Conical Cavities, *J. Appl. Phys.*, **1952**, *23*, 532.
[28] *AUTODYN® Jetting Tutorial*, 3rd Revision, Century Dynamics, USA, **1997**.
[29] Elshenawy T., Li Q.M., Breakup Time of Zirconium Shaped Charge Jet, *Propellants Explos. Pyrotech*., **2013**, *38*, 703.
[30] Elshenawy T., Li Q.M. Influences of Target Strength and Confinement on the Penetration Depth of an Oil Well Perforator, *Int. J. Impact Eng.*, **2013**, *54*, 30.